

# Surface forces in model oil-in-water emulsions stabilized by proteins

Tatiana D. Dimitrova<sup>a,\*</sup>, Fernando Leal-Calderon<sup>b</sup>, Theodor D. Gurkov<sup>c</sup>, Bruce Campbell<sup>d</sup>

<sup>a</sup>Max-Planck-Institute for Polymer Research, Ackermannweg 10, Mainz D-55128, Germany

<sup>b</sup>Institut des Sciences et Techniques des Aliments de Bordeaux, Av. des facultés, Talence cedex 33405, France

<sup>c</sup>Laboratory of Chemical Physics Engineering, Faculty of Chemistry, Sofia University, 1 James Bourchier Ave., Sofia 1164, Bulgaria

<sup>d</sup>Kraft Foods, Inc., Technology Center, 801 Waukegan Road, Glenview, IL 60025, USA

## Abstract

We have employed two complementary techniques, namely, the magnetic chaining technique (MCT) and a variant of the Mysels cell to obtain data concerning the repulsive interaction profiles between protein layers formed at liquid–liquid interfaces. For BSA-stabilized systems, a long-ranged repulsion is operative. It is not of an electrostatic origin, but originates most probably from the formation of multiple protein layers at the interface. The interactions between  $\beta$ -casein layers formed at the water/oil interface are governed by electrostatic repulsion. Due to the relatively large final thickness of approximately 20 nm, the van der Waals contribution to the total disjoining pressure is inferior. The oscillatory component is also negligible for the studied protein concentration of 0.1 wt.%. For both proteins, the extracted information describes the situation where the protein-covered surfaces are approached/manipulated in a quasi-static manner. We observe a very good agreement between the data obtained from MCT and Mysels cell. The comparison of our results with literature data from surface force apparatus (SFA) experiments reveals a substantial difference in the force laws existing between protein-stabilized *liquid* droplets and mica surfaces covered by proteins. We explain this discrepancy in terms of the different protein absorption on solid and liquid interfaces. We also measured the threshold force necessary to induce irreversible flocculation in  $\beta$ -casein and  $\beta$ -lactoglobulin (BLG) stabilized emulsions. Under similar conditions, the threshold flocculation force is higher for  $\beta$ -casein than for BLG stabilized droplets. The flocs formed from BLG covered droplets are tight and remain without visible change for at least 48 h. We speculate that the flocculation is due to formation of protein aggregates between the approaching droplets.

© 2003 Elsevier B.V. All rights reserved.

**Keywords:** Protein-stabilized emulsions; Surface forces; Flocculation; Protein aggregation; Specific interactions

## 1. Introduction

### 1.1. Proteins as emulsion stabilizers

A simple definition of an ‘emulsion’ states that it is a heterogeneous, metastable system, consisting of two immiscible fluids, often referred to as ‘water’ and ‘oil’. One of the phases is dispersed into the other as droplets of colloidal size (i.e. below 100  $\mu\text{m}$ ). The long-term stability is achieved through the coverage of the oil–water interface with amphiphilic molecules. Those are supposed to ensure the kinetic barrier, which prevents the decomposition of the emulsion into water and oil. Protein-stabilized emulsions find a variety of applications in food, cosmetic, and pharmaceutical industry and

provoke considerable scientific interest. The peculiar features of these systems arise mainly from the specific interfacial properties of the stabilizing molecules, i.e. proteins.

Here we would like to emphasize the difference between the stabilization mechanisms operative in the case of low molecular weight surfactants and proteins. The simple emulsifiers significantly lower the interfacial tension and further act [1] via the Marangoni effect, involving lateral diffusion at the interface. The lateral interactions between the adsorbed molecules themselves are considered minimal. The low molecular weight surfactants used in some formulations are non-ionic and generally soluble in both water and oil. As a rule, they are initially dissolved in the continuous phase, and immediately after emulsification a redistribution of the solute between the two phases takes place. This mass-transfer opposes the thinning of the thin liquid films,

\*Corresponding author. Tel.: +31-512-592-298; fax: +31-512-592-561.

E-mail address: tatiana.dimitrova@philips.com (T.D. Dimitrova).

formed between the emulsion droplets, thus ensuring short-run stability [2] of the systems. The stabilizing mechanisms mentioned above are not always operative in the case of protein-stabilized emulsions [3]. It is noteworthy, that proteins do not lower the interfacial tension as much as simple surfactants do, but effective saturation of the surface in this case is reached at molar protein concentrations  $10^3$ – $10^4$  times lower than for the simple surfactants. At higher concentrations in the bulk phase, the surfactants lower the interfacial tension much more than the proteins (consider 13–15 mN/m as the lowest limit of the interfacial tension of protein layers), due to the better packing of the small amphiphiles in the vicinity of the Gibbs dividing plane.

In their bulk solutions, protein molecules maintain a tightly packed structure. Their adsorption at fluid–fluid interface is accompanied by a gradual unfolding, which means that the bio-molecule loses its secondary and higher structure in the adsorbed state. This happens because the presence of a hydrophobic fluid phase (i.e. oil or air) gives the molecule the possibility to minimize the configurational free energy. The adsorbed species are often referred to as denatured or unfolded. This conformation state makes the adsorbed molecules very much different from their non-adsorbed analogues. The process of unfolding uncovers the different segments of adsorbed species and extremely facilitates the lateral interaction between two or more adsorbed molecules. Various interactions are possible, for example ionic, hydrophobic, covalent (disulfide bridging) or hydrogen bonding. As a result, the adsorbed species form a rigid network and the protein layers, which protects the droplets against coalescence are of *nanometer thickness*, viscoelastic, and almost always tangentially immobile. This is a substantial difference with respect to simple surfactants. The large variety of possible interactions as well as the their different time scale make the properties of the protein layers largely dependent on the sample history. This feature is frequently termed ‘aging effects’.

Different workers [4,5] argued that conformation of the protein molecule at the air/water interface differs substantially from that at the oil/water interface. Further studies demonstrated differences in the state of the adsorbed proteins at hydrocarbon/water and at triglyceride/water interfaces [3]. Apparently, the adsorption of proteins at liquid interfaces cannot be considered as a simple occupation of surface sites, and the lucid and convenient concept of ‘end-on’/‘side-on’ orientation, which is frequently used in case of adsorption at solid surfaces, is irrelevant. It becomes also problematic to postulate equilibrium adsorption, because of at least three reasons. Firstly, the existence of many adsorption sites per molecule makes the hypothesis of instantaneous desorption unlikely. Secondly, the denaturation upon adsorption is not reversible, i.e. desorbed species never regain the conformation and structure they obeyed prior

to adsorption. The last, but not the least: it is an experimental fact that reaching constant interfacial tension does not mean reaching constant adsorption. The protein adsorption can continue via multilayer formation [4,6]. The multilayers are constituted by reversibly adsorbed molecules and the surface coverage can be augmented up to 5–10 mg/m<sup>2</sup>.

### 1.2. Modeling of protein stabilized emulsions

The particularities of protein adsorption layers make the examination of the protein-stabilized emulsions tricky, because the real control on the investigating object is not always achieved. The model experiments on emulsions can be divided in two main groups, which we shortly term as macroscopic and microscopic methods. In the first group fall all the model experiments done on bulk quantities of emulsions as, for example, rheology, [7,8] stability against coalescence, [9] sedimentation studies, [10] etc. The advantage is that one obtains useful data for the overall emulsion behavior and evaluates the influence of different factors over size growth, creaming, viscosity, flocculation etc. For example, data from this type of experiment helped for explaining the influence of the total casein content on the resistance of model emulsions against flocculation [11]. Experiments on batch emulsions stabilized with mixed casein allowed a better understanding the role of the protein interfacial composition on the stability of food-type emulsions, [12] etc. The main drawback of this class of methods is that the observed effects result from a sophisticated interplay between various phenomena at different length and time scales. Therefore, a quantitative physical modeling of the behavior of an emulsion is possible only for some special cases.

The experiments from the second group are designed to mimic the interaction between *single drops*. The object under study is the thin liquid film, which separates two droplets. One obtains lifetime(s), drainage properties, disjoining pressure–thickness isotherms, critical capillary pressure necessary for breakage of the film, etc. The idea behind this is that the overall stability of a real emulsion against coalescence and/or flocculation is related to the stability of the single films [1]. Other overall properties like sedimentation stability or rheological behavior are strongly dependent on the extent of flocculation, the tightness on the flocs, and droplet mean diameter, all those being directly related to the properties of the films as well.

When (protein-stabilized) emulsions are mimicked, there are at least three main reasons, which make investigation of emulsion films (instead of foam ones) necessary.

- i. As already discussed, the protein adsorbs in different ways at air/water and oil/water interfaces. This can

influence substantially the surface aggregation and inter-particle interactions between the adsorbed moieties. As a consequence, the surface rheological properties (both dilatational and shear ones) in the two cases differ significantly [13,14]. The rheology of the film's surfaces is important for the lifetime and thinning rate [15].

- ii. The Hamaker constant for air bubbles interacting across an aqueous medium is approximately 10 times larger than the Hamaker constant for hydrocarbon layers interacting across the same water film. Therefore, the stability of the films may change substantially, especially for small thickness, where the van der Waals interactions become important. This argument is valid for all emulsion systems, regardless the stabilizing agent.
- iii. The emulsion films provide the unique opportunity to probe the influence of the mass transfer across the interfaces (i.e. non-equilibrium effects) on the behavior of the studied systems. Even this effect is not supposed to play a major role in systems stabilized solely by proteins; it could be of considerable importance when non-ionic surfactant is present.

Below we shortly consider several types of experiments that allow forming and reliably manipulating model emulsion films. The referenced literature does not cover the whole body of available data, we restrict ourselves to the experimental developments with a (possible) application to protein-stabilized systems.

### 1.2.1. Scheludko cell

Originally designed for studying foam films, the technique has been extended for emulsion films as well. The film is made by sucking the liquid from a biconcave meniscus. The set-up is relatively easy to operate, allows precise determination of the contact angles (i.e. interaction energy between the studied droplets) and offers the possibility video microscopy. The major drawback is the low attainable capillary pressure—approximately 100 Pa. In real emulsions it is much higher – above several thousand Pascals. The capillary pressure,  $P_c$ , is an important parameter because it determines both the radius of the formed film,  $r_f$ , and the rate of its thinning,  $V_{Re}$ . For films with circular symmetry one obtains: [1]

$$P_c = \frac{2\gamma R_c}{R_c^2 - r_f^2 \cos\varphi}, \quad (1)$$

$$V_{Re} = \frac{2h^3 P_c}{3\mu r_f^2}, \quad (2)$$

where  $R_c$  denotes the radius of the capillary cell,  $\gamma$  is the interfacial tension,  $\varphi$  is the three phase contact angle (glass/film phase/hydrophobic phase),  $h$  is the film thickness, and  $\mu$  is the viscosity of the film phase. Eq.

(2) is the well-known Reynolds equation, which is valid for the case of film with non-deformable surfaces [16].

The Scheludko cell may be combined with FRAP (fast recovery after photo-bleaching) technique [17]. In this case, a small quantity of fluorescent dye is introduced on the film surfaces. When the film reaches its equilibrium thickness the dye from a certain spot is pulse-bleached. The recovery of the fluorescence signal is attributed to the lateral diffusion of the dye molecules. One obtains the surface diffusion coefficient of the dye as function of the film phase composition. It was found that there is a correlation between the surface mobility of the dye and the surface rheological properties of protein and mixed protein-surfactant films [17].

### 1.2.2. Miniaturized Scheludko cell

The principle of this cell is almost identical to that described above. Using laser ablation technique, the authors have fabricated a cell in between two sintered glass lamellae. This cell is 10 times smaller than the conventional one. It has been applied for studying emulsion films stabilized by Tween 20 (nonionic surfactant) and Bovine serum albumin (BSA). As expected (see Eq. (2)) the drainage is much faster in comparison with the analogous films formed in the Scheludko cell. The hydrodynamics of the film formation is different as well, being 'thinning' in the case of conventional cell and 'spreading' in the case of miniaturized one. However, this configuration is inconvenient for thickness and contact angle measurements [18].

### 1.2.3. Drop pressed against a large homophase

Some authors investigate the lifetime of the emulsion films formed between a drop pressed against a large homophase by buoyancy [19,20]. The overall dependence of the lifetime on the drop radius passes through a shallow and broad minimum. For small non-deformable droplets no film is formed and the drainage velocity of the liquid layer between the drop and the interface can be described by the Stokes equation, with appropriate account for the viscous resistance (Taylor–Stokes regime). For large deformable droplets, the film lifetime increases with drop radius because larger drops experience larger buoyancy, i.e. one forms larger films whose thinning is slower (see Eq. (2)).

### 1.2.4. Liquid surface force apparatus

In this case, an oil droplet is attached on a capillary, and this assembly is manipulated so that the droplet approaches water–oil interface. At a distance, where the surface forces get important, the droplet is deformed and oil–water–oil film is formed. It is possible to vary the pressure between the drop and the oil phase, i.e. the disjoining pressure inside the film by moving the droplet up and down. The film thickness is determined independently, employing light interferometry. This configura-

tion is supposed to deliver information about the surface interactions in a wide range of distances and pressures. Until now, the set up has found application for surfactant-stabilized systems only [21].

#### 1.2.5. Film trapping technique

This technique allows determination of the barrier of coalescence,  $P_C^R$ , of a micron-sized droplets and a bulk oil phase. An important feature of the technique is the possibility to vary the drop radius as well as to measure reliably very low pressures. For a detailed analysis, the reader is addressed to the paper by Denkov et al. [22].

#### 1.2.6. Mysels cell

This set-up was originally proposed by Mysels [23] and further developed by Bergeron [24]. The film is formed in a porous plate, which allows increasing the maximal attainable pressure up to thousands of Pa. This cell is considered in great detail in the next section where we describe our own modifications, necessary for its application to emulsion films.

#### 1.2.7. Magnetic chaining technique (MCT)

Magnetic chaining technique [25,26] allows to explore the single contacts between the emulsion droplets. It may be considered as a direct link between the single contact experiments and the macroscopic studies. The method (see next section) works with droplets of colloidal size (approx. 0.2  $\mu\text{m}$  in diameter), i.e. at true capillary pressures and with liquid interfaces. A very important feature of it, is the possibility to explore very low levels of forces: down to approximately  $10^{-6}$  N/m. Another advantage of the method is the 'build-in' ensemble averaging over millions inter-droplet contacts.

### 1.3. Aim of this work

There exists relatively little experimental information concerning the surface forces acting in the emulsion films stabilized by proteins. We applied two complementary techniques, i.e. MCT and a version of Mysels cell to measure the forces acting between protein-stabilized emulsion droplets. We also exploit the MCT in a way, which permits to obtain quantitative description the flocculation (threshold flocculation force) in some cases of protein-stabilized emulsions.

## 2. Experimental part

### 2.1. Substances

The proteins—Bovine Serum Albumin, essentially fatty acid free (BSA),  $\beta$ -lactoglobulin (BLG) and  $\beta$ -casein were Sigma products (catalogue numbers A-7511, L-0130, B-6905 lots 102H93101, 91H7005 and 25H9550, respectively). Tween 20 was purchased from

Fisher Scientific (ICI Surfactants product, enzymatical grade, lot 982322). Sodium dodecyl sulfate (SDS) was purchased from Aldrich. All surface-active products were used as received.

The oil used for emulsion preparation in MCT experiments was a ferrofluid, prepared by Ferrofluidics. It is a 10% vol./vol. dispersion of ferromagnetic ( $\text{Fe}_2\text{O}_3$ ) particles in octane. The grains, 10 nm in size, are stabilized against aggregation by 2% wt./vol. oleic acid. It is proven that the particles remain dispersed in the range of magnetic fields applied in the experiment (0–500 G).

Hexadecane used as an oil phase for Mysels cell studies was of analytical grade. It was purchased from Merck and was used as received.

$\text{NaN}_3$  used for prevention of bacterial growth as well as NaCl used for the adjustments of the ionic strength were Merck products. NaCl was baked for approximately 5 h at 450  $^\circ\text{C}$  in order to remove any organic contamination.

All solutions were prepared with water purified by Millipore Milli-Q unit (Resistance 18.2  $\text{M}\Omega\text{ cm}^{-1}$ ) and filtered through 0.22  $\mu\text{m}$  Millipore cut-off filter prior to use. The protein solutions were stored at constant temperature of 23  $^\circ\text{C}$  for no longer than 8 h. When a longer storage was required, we used solutions that contained 0.02 g/l of  $\text{NaN}_3$ .

## 2.2. Experimental techniques

### 2.2.1. Magnetic chaining technique

The set up is schematized on Fig. 1. This technique exploits the properties of paramagnetic monodisperse droplets. The applied field induces a magnetic dipole within each ferrofluid droplet. The interaction between the magnetic dipoles leads to formation of linear arrays of particles (chains), which are parallel to the external magnetic field. At very low droplet volume fractions ( $\phi < 0.1$  vol.%) the chains are only one droplet thick and the droplets in the chains remain well separated. If the chains are illuminated by a white light source, parallel to them, the emulsion appears beautifully colored in the back-scattering direction. These colors originate from Bragg diffraction and provide a straightforward measure of the spacing between droplets within the chains. For perfectly aligned particles at a separation  $d$ , illuminated by incident white light parallel to the chains, the first order Bragg condition reduces to:

$$d = \frac{\lambda_0}{2 n_0} \quad (3)$$

where  $n_0$  is the refractive index of the suspending medium ( $n_0 = 1.331$  for aqueous solutions), and  $\lambda_0$  is the wavelength of the light Bragg scattered at an angle of 180 $^\circ$ . The wavelength corresponding to the maximum

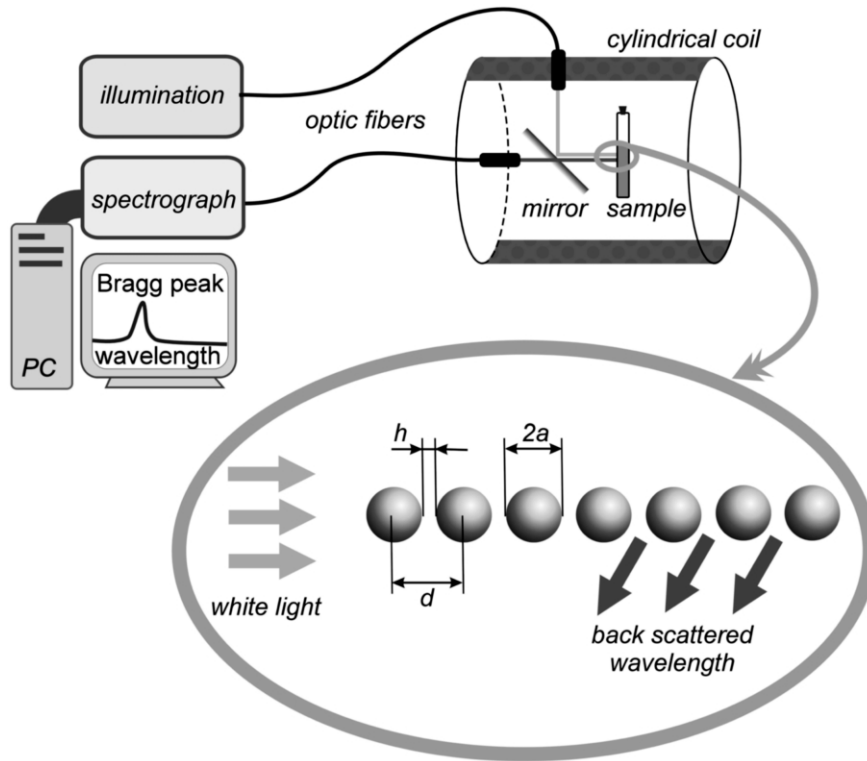


Fig. 1. Schema of the set-up of magnetic chaining technique (not to scale).

of the Bragg peak provides a direct measurement of the average spacing between the drops with a precision of approximately 1.5 nm. Because the drops are non-deformable owing to their large capillary pressure ( $\sim 1$  atm), it is possible to determine the interfacial separation,  $h = d - 2a$ , where  $a$  is the droplet radius.

The repulsive force,  $F_r$ , between the droplets must exactly balance the attractive force between the dipoles induced by the applied magnetic field. Since the dipoles are aligned parallel to the field, this force can be calculated exactly and is given by:

$$F_r = F_m(d) = - \frac{1.202}{2 \pi \mu_0} \times \frac{3m^2}{d^4} \quad (4)$$

where  $\mu_0$  is the magnetic permeability of free space and  $m$  is the induced magnetic moment of each drop. The induced magnetic moment is determined self-consistently from the magnetic susceptibility of the ferrofluid, and the presence of the neighboring droplets. Thus:

$$m = \mu_0 \frac{4}{3} \pi a^3 \chi_S H_T \quad (5)$$

where  $H_T$  is the total magnetic field acting on each drop, and  $\chi_S$  is the susceptibility of a spherical droplet. The total applied field,  $H_T$ , is given by the sum of the external applied field,  $H_{\text{ext}}$ , and the field from the

induced magnetic moments in all the neighboring drops in the chain. This can easily be calculated for an infinite chain, assuming point dipoles, giving:

$$H_T = H_{\text{ext}} + 2 \times 1.202 \times \frac{2m}{4 \pi \mu_0 d^3} \quad (6)$$

This technique allows one to measure interparticle forces as small as  $2 \times 10^{-13}$  N, corresponding to the minimum force required for forming chains.

MCT permits to measure only repulsive interactions, as all ‘thin liquid film’ techniques. In contrast to the Mysels or Scheludko techniques, when using MCT, one has no direct glance on the contact zone of interacting droplets. However, MCT has two very important advantages. First, the technique allows an on-line averaging over the pair interactions (at a given distance) between a very large number of droplets, which is not possible with the other techniques, aimed to model the single contact between two emulsion droplets. Second, there is a possibility to induce flocculation in a controllable way. The latter is possible for flocculation barriers of some  $\mu\text{N/m}$ . We find this possibility interesting and worth exploring.

### 2.2.2. Mysels cell

We developed a version of the Mysels type cell, which allows relatively convenient operations with both

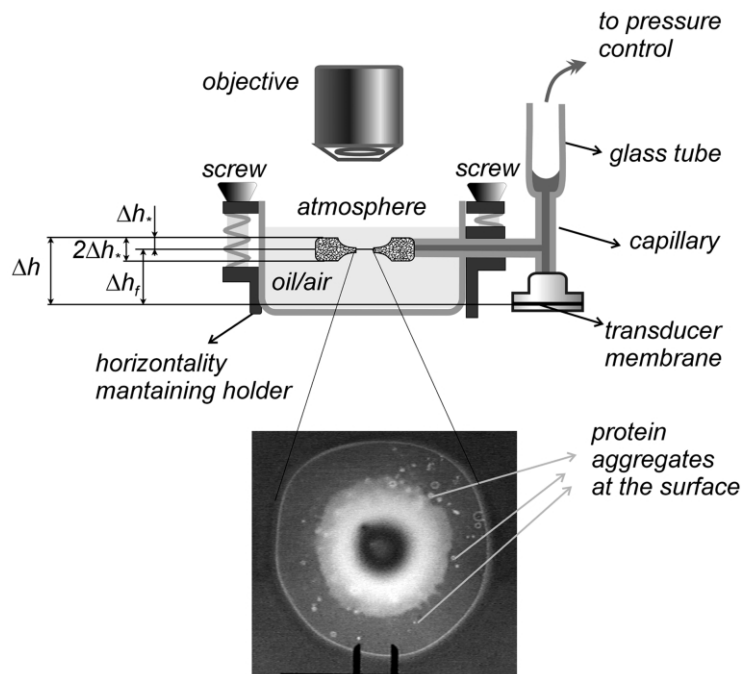


Fig. 2. Operational principle of Mysels cell employed in this study. The photomicrograph shows an example of a BSA stabilized foam film with considerable surface aggregation at ca. 2400 Pa. The foam film was chosen only for the sake of better contrast.

foam, and emulsion films [27]. In the set-up proposed by us (Fig. 2), the film is formed in a circular porous plate by sucking liquid via side mounted capillary. The cell is directly connected to the pressure transducer (Omega PC136–G01 or Omega PC136–G05, depending on the studied pressure range). The reference pressure is the atmospheric one. This configuration provides the opportunity to investigate *both* foam and emulsion films. When the construction shown in Fig. 2 is used, the measured value for the pressure,  $P$ , should be corrected for the hydrostatic pressure difference between the plane of the film and the level of the measuring membrane of the transducer. That difference was obtained by calibration in the following way: the cell was filled up with the appropriate aqueous phase to the point where the upper edge of the porous plate is exactly at the level of the aqueous phase. The measured pressure is:

$$P = \Delta\rho g \Delta h = \Delta\rho g \Delta h_f + \Delta\rho g \Delta h_*, \quad (7)$$

where  $\Delta\rho$  is the density difference between water and air, and the heights  $\Delta h$ ,  $\Delta h_f$  and  $\Delta h_*$  are shown in Fig. 2. The value  $2\Delta h_*$  can be measured directly with sufficient precision; thus,  $\Delta h_f$  is determined from Eq. (7). Let us now consider the situation where a film is formed. If in the system of Fig. 2 the big vessel containing the cell is filled up with oil (aqueous emulsion films), then the real capillary pressure,  $P_c$ , is given by the following relation:

$$P_c = -P_m + \Delta\rho g \Delta h_f + \Delta\rho_1 g \Delta h_* \quad (8)$$

Here  $P_m$  is the measured pressure, and  $\Delta\rho_1$  is the density difference between oil and air. All other symbols are the same as above. Note that the lower the pressure the higher the relative contribution of the corrections. The cell is open to the atmosphere, which is very convenient from a practical point of view, especially when studying emulsion films. For foam films the term with  $\Delta\rho_1$  in Eq. (8) will vanish. In this case, 2 ml of the corresponding protein solution is placed in the bottom of the big vessel (total volume ca. 20 ml) and the latter is covered by a glass slide. This is done in order to saturate the vapor pressure inside the chamber, thus preventing the evaporation from the film phase. The whole construction is made out of glass, which permits an easy and reliable cleaning with respect to surface-active material.

The cell is attached on the table of an Axioplan Zeiss Microscope. The film thickness is determined via standard interferometry. Therefore, the film has to be strictly horizontal. The intensity of the reflected light is connected with the film thickness via the expression:

$$h = \frac{\lambda}{2\pi n_0} \left( k\pi + \arcsin \sqrt{\frac{I - I_{\min}}{I_{\max} - I_{\min}}} \right), \quad (9)$$

where  $I_{\max}$  and  $I_{\min}$  denote the maximal and minimal intensity of the reflected light, respectively (measured by means of a photo-multiplier tube),  $k=0,1,\dots$  is the order of the interference maximum,  $\lambda$  is the wavelength of the incident light (546 nm) and  $n_0$  is the refractive

index of the liquid forming the film. This formula neglects the interfacial layers, giving, as in the case of MCT, the so-called ‘equivalent water thickness’. This is important for the further comparison of the results obtained by both methods. We always consider the equivalent water thickness, because physical properties of the protein layers are strongly dependent on the sample history. The literature data for the thickness and refractive index of the protein layers are not always consistent and the adoption of ‘sandwiched’ models, like in Ref. [24], cannot be justified.

The reliability of the set up is tested on foam films stabilized with the non-ionic surfactant Tween 20. The disjoining pressure vs. distance isotherm is very well described by the classical electric double layer interaction combined with oscillatory repulsion [27]. The latter arises from the exclusion volume effect of the surfactant micelles.

We have the possibility to evaluate disjoining pressure vs. thickness isotherms,  $\Pi(h)$  for emulsion films. However, special care has to be taken when attaching the pressure transducer to the glass part. Entrapment of air bubbles causes severe errors in pressure determination because the gases are compressible. There are some other sources of artifacts as well. First, proteins adsorb on the glass surfaces and may render the latter hydrophobic. This is observed for BSA and sometimes for BLG. As a consequence, the film frequently detaches from the cell and ruptures at very low disjoining pressure. Another crucial point is the regularity of the film surface. Light scattering experiments show that there is no clustering in the bulk protein solutions of BSA and BLG. However, the protein-stabilized films exhibit in both cases surface clustering [10,27,28]. An example is present in Fig. 2, where we show a BSA stabilized film, containing aggregates. The fact that these aggregates are ‘surface born’ has been recently confirmed by Brewster angle microscopy experiments performed on interfacial layers of BLG and whey protein isolate (WPI) [29].

The interferometric method for thickness determination is applicable only to perfectly plane-parallel films, therefore it is necessary to work on aggregate-free films only. After a few films (say maximum 3) have formed and ruptured, the aggregation becomes considerable. Therefore, we paid special attention to work only with the first one or two films, formed after loading the two phases into the cell. We consider the surface aggregation as a considerable issue we shall discuss this point below.

A few Mysels type cells were used in the experiments. They differ in the size of the pores, i.e. in the maximum attainable capillary pressure. For each system we co-plotted the data from different runs and fitted these common plots.

### 2.2.3. Auxiliaries

*Preparation of ferrofluid-in-water emulsions for MCT.* The primary crude ferrofluid-in-water emulsion was prepared according to the method of emulsification in viscoelastic media developed by Mason and Bibette [30]. As emulsifier we used SDS. This technique leads to relatively narrow sized droplet distributions, but not sufficient for the applied force measurement technique. So, the emulsion was diluted with  $1 \times \text{CMC}$  SDS solution ( $\text{CMC} = 0.008 \text{ M}$ ) and further refined following a fractionation crystallization procedure similar to that suggested by Bibette [31]. At least 6–7 steps were necessary to obtain an emulsion with sufficient degree of monodispersity. The size of the droplets was determined by dynamic light scattering measurement (performed by means of a Brookhaven correlator). We found a mean diameter of 178 nm and polydispersity of approximately 5%.

This SDS-stabilized emulsion was further treated in order to cover the interfaces with the chosen surface-active molecules. This was achieved applying the so-called washing procedure, which consists of concentrating the emulsion by means of centrifugation, followed by replacing the supernatant with a new aqueous phase, which contains the desired surfactant. When the process is repeated a few times, only negligible traces of the primary surfactant (SDS) are left at the droplet interface. It is also necessary to ensure *no change* of the size distribution and no effects like flocculation and coalescence. Replacing the surfactant with a protein is tricky, because the surfactants (especially the ionic ones) have a strong tendency to bind to the proteins, causing unfolding, formation of complexes, etc. For that reason, it was necessary to exchange the SDS with a non-ionic surfactant before adding the protein. We chose Tween 20, which is a common, widely studied non-ionic surfactant with a low CMC. After the coverage of the emulsion droplets with Tween 20 is achieved, we continue the washing process in the same way in order to adsorb BSA,  $\beta$ -casein or BLG on the interface.

*Electrophoretic mobilities* of the emulsions were measured using a Malvern Zetasizer II. The electrophoretic mobility was transformed into  $\zeta$ -potential according to the Smoluchowski equation [15].

*pH control.* The pH values were measured by means of a digital pH-meter, equipped with protein and surfactant resistant electrode.

The proteins obey buffering properties. When dissolved in water, they generally maintain certain pH value (which may depend on the purification process), frequently referred to as ‘natural pH’. This property of the proteins was used in our experiments to control the pH. For each protein ( $\beta$ -casein, BSA, BLG) we verified that the pH is constant within 0.2 units over the range of concentrations studied. No drift of the pH values of

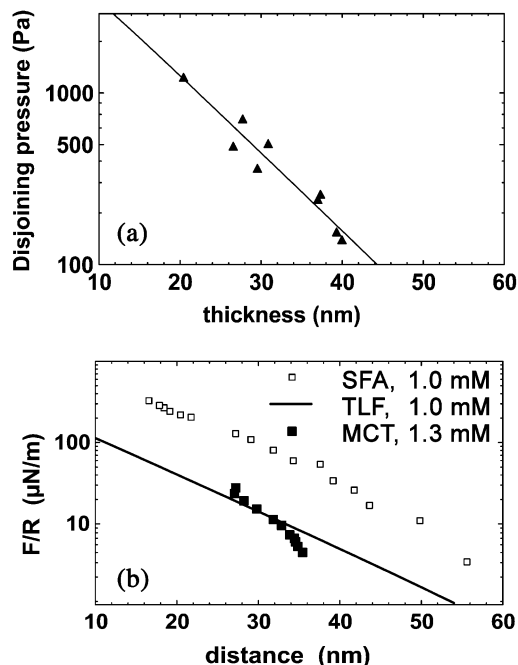


Fig. 3. (a) Disjoining pressure vs. thickness isotherm (dots-experimental data, line -DLVO fit) for an emulsion film stabilized by 0.1%  $\beta$ -casein, ionic strength of 1 mM NaCl, oil phase-hexadecane. (b) Comparison between the data obtained from TLF, MCT and SFA.

the protein solutions was observed over the period of storage (8 h).

We chose this way to maintain the pH and did not use a conventional buffer solution because buffers contribute to the total salt content (i.e. the ionic strength) and this significantly narrows the available range of ionic strengths.

All glassware, including the cells for film formation, was soaked for 20 min in concentrated chromic–sulfuric acid, then thoroughly rinsed with abundant quantities of Millipore purified water and finally dried at 50 °C in a closed oven.

### 3. Results

#### 3.1. Force–distance measurements

##### 3.1.1. $\beta$ -casein

Employing the Mysels cell, we measured the disjoining pressure vs. thickness isotherms of thin liquid films (TLF) between hexadecane droplets stabilized by 0.1 wt.%  $\beta$ -casein. The pH was 6.1, the ionic strength was fixed by 0.001 M NaCl. In this case, we find a DLVO behavior. Fig. 3a shows the experimentally obtained  $\Pi(h)$  isotherm (dots) and the best DLVO-fit (Eq. (10)). The fit is done supposing constant surface potential,  $\Psi_s$ ; the plane of charge is taken to coincide with the water/oil interface. The value of the Hamaker constant,  $A_H$ , is  $0.49 \times 10^{-20}$  J. The Debye length,  $\kappa$ , is calculated

from the electrolyte concentration,  $C_{el}$ , (Eq. (11)):

$$\Pi_{DLVO} = -\frac{A_H}{6\pi h^3} + 64 C_{el} kT \tanh^2\left(\frac{e\Psi_s}{4kT}\right) \exp(-\kappa h) \quad (10)$$

$$\kappa(\text{nm}^{-1}) = 3.29 \sqrt{C_{el}(\text{mol/l})} \quad (11)$$

The only free parameter is the surface potential, which is found to be  $-27.8$  mV. It agrees fairly well with the data in the literature [32] ( $-30$  to  $36$  mV) for the  $\zeta$ -potential of  $\beta$ -casein covered particles. Since casein is reported in the literature to form micelle-like aggregates of various sizes, it is important to estimate the magnitude of the oscillatory structural forces. Taking the average diameter of the  $\beta$ -casein aggregates (micelles) to be 26 nm [33] and 250 kDa [12] for their molecular mass, one calculates exactly [15] the contribution of the oscillatory disjoining pressure to the measured pressure. The calculations show that the volume fraction of the micelles is less than 2% and the oscillatory pressure exerted by them is of the order of magnitude of the experimental uncertainty in the pressure determination.

It is interesting to compare these data with the output of MCT and surface force apparatus (SFA). This requires a conversion of the disjoining pressure in energy per unit area. By analytical integration over the thickness of the expression for the disjoining pressure (taking for  $\Psi_s$  the value provided by the best fit) one obtains the corresponding energy per unit area,  $f(h)$ , between two infinite planes: [15]

$$f(h) = \int_h^\infty \Pi(h) dh \quad (12)$$

Adopting the Derjaguin approximation one can find the real force,  $F(h)$ , acting between two spheres of equal radii, which is exactly the quantity measured in the MCT experiments:

$$F(h)/a = \pi f(h) \quad (13)$$

In Eq. (13),  $a$  is the radius of the spheres. For crossed cylinders of the radius of curvature  $R$  one obtains:

$$F(h)/R = 2\pi f(h) \quad (14)$$

The comparison is plotted in Fig. 3b. The SFA data were taken from the literature [34]. They have been obtained for hydrophobised mica surfaces, protein concentration of 0.01 wt.%, ionic strength of 0.001 M, and pH 7. Evidently TLF and MCT lead to very similar results, which permit us to state that under these conditions the electrostatic repulsion is the main force governing the behavior of the studied system. The comparison with the SFA data demonstrates that the



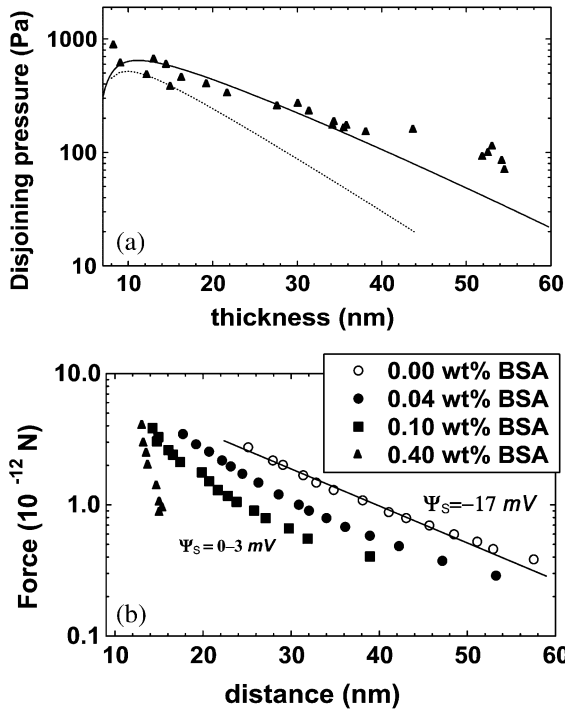


Fig. 4. (a) Disjoining pressure vs. thickness isotherm for an emulsion film stabilized by 0.1% BSA, ionic strength of 1 mM NaCl, oil phase-hexadecane. The dots are the experimental data, dashed line is the DLVO contribution to the total disjoining pressure, and the solid line is the best fit done supposing additivity of the DLVO and steric forces. (b) Force vs. distance profiles for ferrofluid emulsions stabilized with mixed BSA-Tween 20 adsorption layers. The total concentration of the Tween 20 is kept constant- $5 \times \text{CMC}$ , pH 5.8.

force laws are only qualitatively similar. This is more or less expected, since the protein layers formed in the two types of experiments are incompatible, due to the substantial differences in the conformation at the two types of surfaces. The difference between the values is approximately 1 decade. This result strongly suggests that extrapolation of the data concerning the forces between protein layers formed on a surface of a given type to another surface cannot be always justified.

### 3.2. BSA

For the TLF experiments we worked with 0.1 wt.% BSA solutions. The ionic strength is 0.001 M NaCl, and pH of  $5.7 \pm 0.1$  (natural). The oil phase is again hexadecane. The results from the Mysels-type cell are shown as points in Fig. 4a.  $\zeta$ -potentials of hexadecane droplets, covered by BSA, measured under similar pH and salt conditions [35] provide values between  $-5$  and  $0$  mV. Hence, we use  $-10$  mV for the surface potential in order to estimate the maximal DLVO-contribution to the total disjoining pressure (dashed line in Fig. 4a). As in the case of  $\beta$ -casein  $A_H = 0.49 \times 10^{-20}$  J and the Debye length is 9.6 nm (corresponding to 1 mM 1:1

electrolyte). Apparently, the measured repulsive pressure is longer-ranged compared to the one predicted by the DLVO model. This means that there is an additional repulsive interaction, which remains not captured by the theory. It is established in the literature [36,37] that BSA layers exhibit strong and long ranged, steric repulsion, so it is natural to expect such interactions to be present in our films. For numerous proteins it is known that after reaching the equilibrium interfacial tension (for a certain protein concentration) the adsorption,  $\Gamma$ , continues to increase [4,6]. The latter fact is attributed to the formation of extra surface protein layer(s) of partially unfolded protein molecules. To take into account the formation of the second protein layer(s) one may use the approach of Israelachvili and Wennerström [38]. The idea is to derive an expression for the disjoining pressure exerted by ‘ordering’ of BSA entities just under the dense interfacial protein layer. Supposing the density,  $\rho(z)$ , of the sub-surface layer(s) decreases exponentially with the distance,  $z$ , from the interface, we can write:

$$\rho(z) = \rho(z_0) \exp(-h/\lambda^*) \quad (15)$$

where  $\lambda^*$  is the characteristic size of the protein species that constitute the second layer(s). We neglect the correlations between the moieties in the sub-surface layer and consider the case when two surfaces approach each other. Imposing non-overlapping of the protein sub-layers, one obtains the following expression for the repulsive pressure: [38]

$$\Pi_{\text{repulsion}}(h) = \frac{\Gamma_2(kT/\lambda^*)(h/\lambda^*)\exp(-h/\lambda^*)}{1 - (1 + h/\lambda^*)\exp(-h/\lambda^*)}, \quad (16)$$

where  $\Gamma_2$  is the adsorption in the second (sub-surface) protein layer only. For distances larger than the characteristic size of the protein species forming the sub-layer, Eq. (16) reduces to:

$$\Pi_{\text{repulsion}}(h) = \Gamma_2(kT/\lambda^*)(h/\lambda^*)\exp(-h/\lambda^*) \quad (17)$$

Assuming additivity of the DLVO pressure (Eq. (10)) and the repulsive steric pressure Eq. (17), we fit our experimental data using as free parameters  $\Gamma_2$  and  $\lambda^*$  (solid line in Fig. 4). The values obtained are  $0.23 \text{ mg/m}^2$  and  $10.7 \text{ nm}$ , respectively. From a physical point of view these values are quite reasonable. An increase of the total adsorption (after the equilibrium value of the surface tension is reached) of approximately  $0.5 \text{ mg/m}^2$  is reported in the literature [39]. This is exactly what  $\Gamma_2$  stands for in model. The value of  $\lambda^*$  is consistent with the size of the BSA molecule ( $11.4 \times 11.4 \times 4.1 \text{ nm}$ ), as well as with the radius of gyration of a BSA molecule of  $\sim 9 \text{ nm}$ .

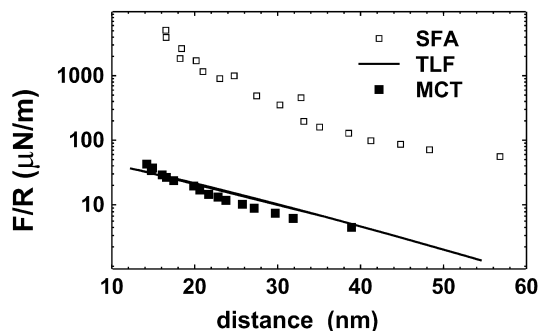


Fig. 5. Comparison between the data obtained from TLF, MCT and SFA for systems stabilized with BSA. See text for details.

We consider now the MCT experiments. In all our attempts to wash the emulsions with ‘pure’ BSA we always obtain flocculated samples. When all Tween 20 is removed, the droplets flocculate and form large clusters. Therefore, it was necessary to prevent the flocculation of the samples by adding traces of Tween 20.

We perform a set of measurements in which we varied the Tween 20 and BSA concentrations over a wide range. At constant Tween 20 concentration, when the protein content is increased from 0 to 0.4 wt.%, there is a progressive change with respect to classical double-layer repulsion. Typical results are shown in Fig. 4b, where the Tween 20 concentration is kept at  $5 \times \text{CMC}$ . For pure Tween 20, the repulsion profile is fitted by standard DLVO curve, yielding a surface potential of  $-17$  mV, which is in very good agreement with the  $\zeta$ -potential of the droplets [8]. The profiles in the presence of the same quantity of BSA at surfactant content of  $20 \times \text{CMC}$  and  $50 \times \text{CMC}$  are very similar and do not depend on the Tween 20 concentration as well [8]. This suggests that the presence of the protein dominates the behavior and the properties of these systems.  $\zeta$ -potential measurements of these droplets gave values of 0–3 mV, meaning that the contribution of the electrostatics to the total repulsive force is negligible. This result undoubtedly shows that the operative repulsion, which we register, is due to specific (non-DLVO) interactions.

Bearing in mind this remark we compare the data from the Mysels cell experiments with those from MCT in Fig. 5. The disjoining pressure is transformed into force in the same manner as in the case of  $\beta$ -casein and compared with data from MCT and SFA [40]. The data from MCT and TLF show reasonably good agreement. The results from the SFA studies are only qualitatively similar to both MCT and TLF data. The reason is essentially the same as in the case of  $\beta$ -casein-stabilized films, i.e. the difference in the conformational state of BSA on solid–fluid and on fluid–fluid interfaces.

### 3.3. Threshold flocculation force

During the preparation of the samples for MCT, we observed a very strong dependence of the properties of emulsions on the history of preparation. In some cases the emulsions were irreversibly flocculated during the washing steps. The flocculation is always observed after centrifugation, i.e. when the droplets are brought in contact. As already discussed, it was impossible to produce non-flocculated droplets stabilized solely with BSA. For the cases of BLG and  $\beta$ -casein it is possible to produce non-flocculated emulsions stabilized by the protein only, however, these systems show the same tendency to flocculate when centrifuged at acceleration bigger than  $150\text{--}200 \times g$ . We use this fact for determination of the threshold flocculation force employing the MCT in the following way.

The investigated sample was submitted to a magnetic field. We registered the force and inter particle distance, as described in Section 2.2.1 and switch off the magnetic field. Then we observed the emulsion under microscope. The removal of the magnetic field is expected to lead to instantaneous decomposition of the formed chains. This is observed for ferrofluid oil in water emulsions stabilized by low molecular weight surfactants [25,26]. For the proteins studied here, we observe under microscope that above some critical force, the droplets remained irreversibly chained even in the absence of a magnetic field. Fig. 6 shows the force profiles for ferrofluid oil-in-water emulsions stabilized by 0.1 wt.% protein at various ionic strengths. When the droplet surfaces were covered by  $\beta$ -casein, we observe standard DLVO behavior up to a force,  $F^*$ , above which droplets are held together in flexible chains that persist in time. Importantly,  $F^*$  is lower than the force corresponding to the maximum of the repulsive barrier. The dashed lines in Fig. 6a are the best DLVO fits with a detailed account for the exclusion volume effect of  $\beta$ -casein micelles. The dependence of  $F^*$  on the ionic strength is shown in Fig. 6c. The decrease in the resistance against flocculation when the ionic strength increases may be due to the screening effect of salt. As far as we know, values of that kind are the first directly measured.

We tried to measure also the forces between droplets, covered by BLG. We were able to measure only low forces, since the application of forces as small as 1 pN lead to irreversible flocculation of the emulsion droplets. In fact, the quality of the Bragg peaks in this case is very low. The latter results in a big uncertainty in the distance determination. A bad quality diffraction pattern may come either from non-perfect alignment of the droplets in chains or from the large polydispersity. We should admit that some small flocs (containing two or three droplets) are observed even after the first washing cycle. A few typical force profiles are shown in Fig. 6b, where the concentration of the protein in the continuous

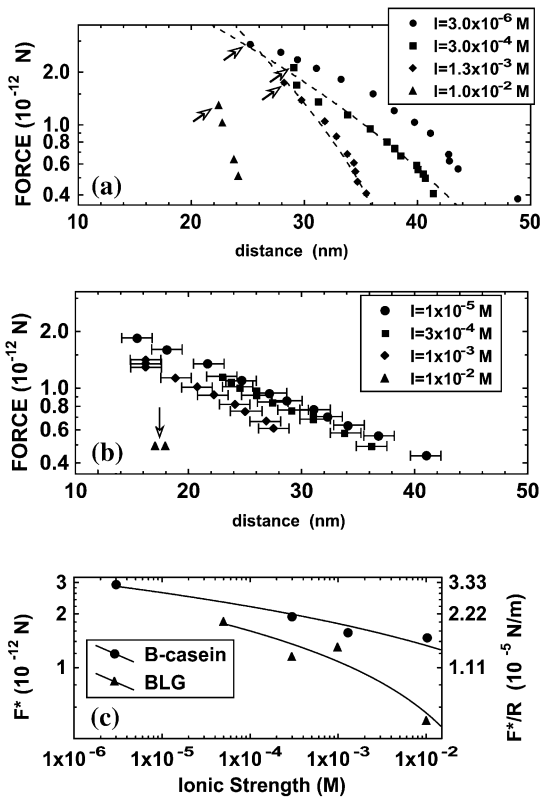


Fig. 6. (a) Force vs. distance profiles for ferrofluid emulsions stabilized with 0.1 wt.%  $\beta$ -casein at pH 6.2 and at different ionic strength (points). The lines (where presented) are the best fits. (b) Force vs. distance profiles for ferrofluid emulsions stabilized with 0.1 wt.% BLG at pH 6.0 and at different ionic strengths. (c) Threshold flocculation force for ferrofluid oil-in-water emulsions stabilized with  $\beta$ -casein and BLG as a function of the ionic strength. The lines are guides for the eye.

phase is 0.1 wt.%, and the ionic strength is varied from  $5 \times 10^{-5}$  to  $1 \times 10^{-2}$  M. The pH of the samples is  $6.0 \pm 0.1$ . No force profile is really measured for ionic strength of  $1 \times 10^{-2}$ . The emulsion flocculates irreversibly at the lowest applied force of ca. 0.5 pN. One anticipates that the electrolyte makes the force shorter ranged, (as expected in the framework of the conventional double-layer repulsion). Because of both distance uncertainty and narrow force range we do not make any attempts to fit these experimental data. Evidently, the threshold flocculation force, plotted in Fig. 6c refers to the irreversible chaining and has to be considered as an upper limit.

Fig. 6c suggests that the critical threshold flocculation force (under equivalent conditions) is lower for BLG-stabilized emulsions. The effect is more pronounced for higher ionic strength. These results are inline with experiments on bulk quantities of micron sized emulsions stabilized by BLG and  $\beta$ -casein. While the BLG-stabilized samples are almost always flocculated (tight flocs are observed), the flocculation in the  $\beta$ -casein case

(under similar experimental conditions) is transient, with temporarily existing flocs [10].

Another interesting phenomenon is observed for BLG-stabilized system. The droplets are so tightly joined that the ‘irreversible’ chains are linear rods that remain unchanged for a period as long as 48 h. The chains formed by  $\beta$ -casein stabilized particles are rather flexible and tend to decompose for the same period of time. An example is shown in Fig. 7, where we present optical micrographs of a BLG-stabilized emulsion. Application of a magnetic field corresponding to a force of 1 pN leads as expected to a formation of chains, which are oriented parallel to the field. The imperfections in the chains (arrows in Fig. 7a) are most probably small clusters comprising several droplets. Such clusters are not present in the original emulsion before the introduction of BLG. They appear during the process of replacement of Tween 20 with BLG. The ‘grains’ in the chains explain the low quality of the Bragg peaks.

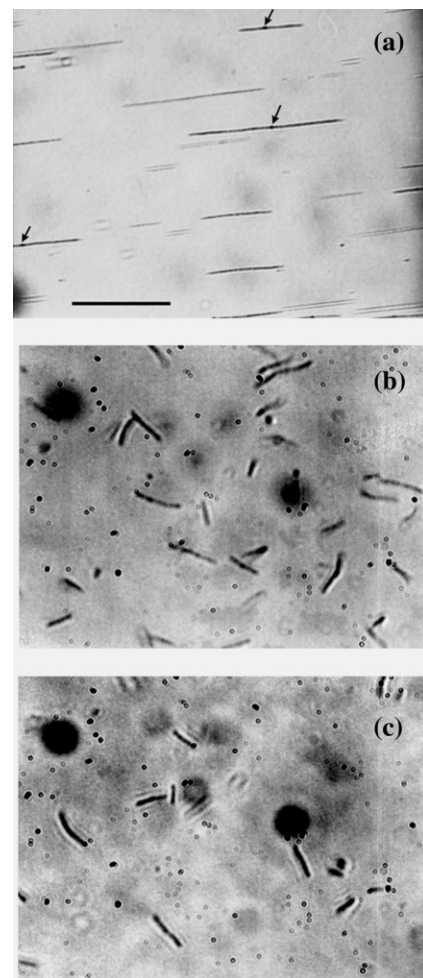


Fig. 7. Optical micrographs of a ferrofluid oil-in-water emulsion stabilized by 0.04% BLG. The bar corresponds to 10  $\mu$ m. (a) on field corresponding to force of ca. 5 pN. (b) ca. 30 min after switching off the magnetic field. (c) 24 h after switching off the magnetic field.

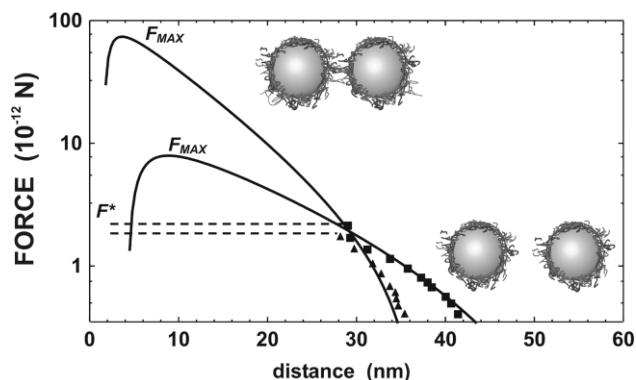


Fig. 8. Flocculation induced by the interaction between the adsorbed protein layers. The data are the same as in Fig. 6a, the Y-scale is chosen to show the repulsive profiles as obtained from the best fit. The thickness of the protein layers is exaggerated.

After removal of the field (Fig. 7b) the chains do not decompose, and we observe rigid rods, which stay the same even after 24 h (Fig. 7c). The existence of these rods suggests that the contacts between the individual droplets, forming the chains are substantially strong and cannot be affected by the thermal motion (i.e. energy of the order of  $kT$ ). The dark dots in Fig. 7b,c are smaller flocs, comprising a few droplets. The images look somehow out of focus, which is due to the fact that the investigated objects are small. Both the rods and the tiny flocs are close to the resolution limit of the optical microscopy and are constantly moving due to the Brownian motion.

#### 4. Discussion

The measurements of the force–distance profiles, together with the threshold flocculation force may explain some of the discrepancies which are frequently observed between the ‘single film’ studies and the behavior of bulk emulsions. The output of the ‘single film’ studies is always repulsive potentials: This is also the case in the present work. However, there are numerous experimental observations of irreversibly flocculated micron-sized droplets [10]. Based on the experiments described above, we propose the following physical picture. When the droplets are apart from each other, in a way that the two protein layers are not in contact, the operative laws are long-ranged repulsive forces of various origin. This is what we measure employing the MCT and the Mysels cell. Fig. 8 provides a graphical guidance. This is the same plot as Fig. 6a, but the Y-scale is chosen so, that the maximum repulsion force is shown. When droplets get closer, the approaching pro-

tein layers start ‘touching’ each other. This allows some of the adsorbed entities to interact forming a local link. We emphasize that these are *point-like contacts* due to interactions at molecular scale. We have termed these links ‘surface aggregates’ because in the thin liquid film experiment as well as in Brewster angle microscopy studies, [29] the biggest of them appear like lumps of material located on the surface. We stress again that those lumps appear on the interface as a result of rapid surface distortion. They are not a product of bulk interactions [29]. AFM images of  $\beta$ -casein and BLG layers formed at water-tetradecane interface and further transferred on mica by Langmuir–Blodgett technique, reveal a network formed by the adsorbed species [41]. This is a further evidence for the interaction between the proteins in the adsorbed state. The network formation is possible because the adsorbed proteins are unfolded (denatured) and therefore segments of various types are available for interaction. Evidently, a distortion of a protein layer will generate more interaction sites. This explains why we observe increasing number of aggregates each time a new film is formed in the Mysels cell. Provided that two protein-covered droplets are sufficiently close, there is no difference whether the interacting entities belong to the same or to different protein layers.

This interaction of the adsorbed species is a local spontaneous process; therefore it cannot be captured by the classic mean-field theories (like DLVO for example). The latter consider the stabilizing layers as uniform. This assumption fails when two protein layers come at a distance, which allows spontaneous local interactions. Therefore, the value of the critical flocculation force, measured above, has to be considered as the force necessary to bring the droplets at the minimum distance allowing for the formation of surface clusters between the two protein layers. This is the reason why  $F^*$  is lower than the maximum repulsive force, predicted by the model.

The flocculation is irreversible when the thermal energy (some  $kT$ ) becomes insufficient to disjoining the aggregates.

#### 5. Conclusions

The experiments employing the magnetic chaining technique (MCT), as well as our variant of the Mysels cell permitted to obtain data concerning the repulsive branch(es) of the interactions between protein layers formed at liquid–liquid interfaces. For BSA-stabilized systems, a long-ranged repulsion is operative. It is not of an electrostatic origin, as both experiment and calculations proved. It most probably originates from the formation of multiple protein layers at the interface, an effect that is well documented in the literature. The interactions between  $\beta$ -casein layers formed at the water/hexadecane interface are governed by electrostatic

repulsion. Due to the relatively large final thickness of approximately 20 nm, the van der Waals component of the total disjoining pressure is negligible. The oscillatory component of the disjoining pressure is also very small for the studied protein concentration of 0.1 wt.%. However, our previous studies [8] have revealed that the onset of the exclusion volume effect due to the  $\beta$ -casein micelles can be detected at similar concentrations.

MCT and Mysels cell experiments are very delicate in general, and we emphasize that in both cases the extracted information refers to the situation where the protein-covered surfaces are approached/manipulated in a quasi-static manner. The latter was found to be a necessary prerequisite to obtain layers free from surface aggregates.

Our experiments reveal a substantial difference between the pertinent force laws existing between protein-stabilized *liquid* droplets (measured both with MCT and Mysels cell) and mica surfaces covered by proteins (literature data from SFA experiments). This result can be justified considering the difference of the protein conformation on solid and liquid interfaces.

We also employed the MCT for determining the threshold flocculation force in the case of  $\beta$ -casein and BLG stabilized emulsions. Importantly, the flocculation is due to the formation of local aggregates between the approaching droplets, rather than the overcome of a repulsive barrier. Our results suggest that the critical threshold flocculation force (under equivalent conditions) is the lower for BLG. Furthermore, the flocs comprising BLG-covered droplets are more rigid than the flocs formed from  $\beta$ -casein stabilized droplets.

## Acknowledgments

This work was mainly done in Centre de Recherche Paul Pascal, Pessac, France and LCPE, Sofia. It was financially supported by a Ph.D. scholarship from Laboratoire Franco-Bulgare (TDD) and partially by Kraft General Foods. The stay in MPIP of TDD was possible through a Marie Curie Fellowship of the European Community program 'Human Potential' under contract number HPMF-CT-2001-01188. The authors are indebted to Dr Asen Hadjiiski for fruitful discussions as well as to Ms Nikolina Vassileva for the assistance in some of thin films experiments.

## References

- [1] I.B. Ivanov, D.S. Dimitrov, in: I.B. Ivanov (Ed.), *Thin Liquid Films*, Marcel Dekker, New York, 1988, Chapter 7 and references therein.
- [2] T.D. Gurkov, K.D. Danov, O.D. Velev, I.B. Ivanov, R.P. Borwankar, *Proceedings of the Second Congress on Emulsion*, 1997, 2, 2-3-155.
- [3] D.G. Dalgleish, *Curr. Opin. Colloid Interface Sci.* 2 (1997) 573.
- [4] D.E. Graham, M.C. Phillips, *J. Colloid Interface Sci.* 70 (1979) 403, 415, 427.
- [5] A.V. Makievski, R. Miller, V.B. Fainerman, J. Krägel, R. Wüstneck, in: E. Dickinson, J.M. Rodríguez Patino (Eds.), *Food Emulsions and Foams Interfaces, Interactions and Stability*, Royal Society of Chemistry, Cambridge, 1999, p. 269.
- [6] T. Sengupta, L. Razumovsky, S. Damodaran, *Langmuir* 15 (1999) 6991.
- [7] G.A. van Aken, T. Vliet, *Langmuir* 18 (2002) 7364.
- [8] T.D. Dimitrova, F. Leal-Calderon, *Langmuir* 15 (1999) 8813.
- [9] S. Tcholakova, N.D. Denkov, I.B. Ivanov, B. Campbell, *Langmuir* 18 (2002) 8960.
- [10] T.D. Dimitrova, T.D. Gurkov, N.D. Vassileva, B. Campbell, *J. Colloid Interface Sci.* 230 (2001) 254.
- [11] E. Dickinson, Y. Matsumura, *Int. J. Biol. Macromol.* 13 (1991) 26.
- [12] E. Dickinson, M. Golding, M.J.W. Povey, *J. Colloid Interface Sci.* 185 (1997) 515.
- [13] B.S. Murray, M. Færgemand, M.M. Trottereau, A. Ventura, in: E. Dickinson, J.M. Rodríguez Patino (Eds.), *Food Emulsions and Foams Interfaces, Interactions and Stability*, Royal Society of Chemistry, Cambridge, 1999, p. 223.
- [14] J. Benjamins, E.H. Lucassen-Reynders, in: D. Möbius, R. Miller (Eds.), *Proteins and Liquid Interfaces*, Elsevier Science, Amsterdam, 1998, p. 341.
- [15] P.A. Kralchevsky, K.D. Danov, N.D. Denkov, in: K.S. Birdi (Ed.), *Handbook of Surface and Colloid Chemistry*, CRC Press, Boca Raton, 1997, Chapter 11 and references therein.
- [16] A. Scheludko, *Kolloid-Z* 155 (1957) 39.
- [17] (a) D.C. Clark, P.J. Wilde, in: D. Möbius, R. Miller (Eds.), *Protein at Liquid Interfaces*, Elsevier, Amsterdam, 1998, p. 267  
(b) P.J. Wilde, M.R. Rodríguez Niño, D.C. Clark, J.M. Rodríguez Patino, *Langmuir* 13 (1997) 7151.
- [18] O.D. Velev, G.N. Constantinides, D.G. Avraam, A.C. Payatakes, R.P. Borwankar, *J. Colloid Interface Sci.* 175 (1995) 68.
- [19] E.S. Basheva, T.D. Gurkov, I.B. Ivanov, G.B. Bantsev, B. Campbell, R.P. Borwankar, *Langmuir* 15 (1999) 6764.
- [20] E. Dickinson, B.S. Murray, G.J. Stainsby, *J. Chem. Soc., Faraday Trans.* 84 (1988) 871.
- [21] B.P. Binks, W.-G. Cho, P.D.I. Fletcher, *Langmuir* 13 (1997) 7180.
- [22] N. Denkov, S. Tcholakova, I. Ivanov, B. Campbell, *Proceedings of the Third World Congress on Emulsions*, 2002, 3-B-198.
- [23] K. Mysels, A. Jones, *J. Phys. Chem.* 68 (1964) 3441.
- [24] V. Bergeron, Ph.D. Thesis University of California, Berkeley, 1993.
- [25] F. Leal-Calderon, T. Stora, O. Mondain-Monval, P. Poulin, J. Bibette, *Phys. Rev. Lett.* 74 (1994) 2959.
- [26] O. Mondain-Monval, F. Leal-Calderon, J. Bibette, *J. Phys. II Fr.* 6 (1996) 1313.
- [27] T.D. Dimitrova, F. Leal-Calderon, T.D. Gurkov, B. Campbell, *Langmuir* 17 (2001) 8069.
- [28] T.D. Gurkov, K.G. Marinova, A.Z. Zdravkov, C. Oleksiak, B. Campbell, *Prog. Colloid Polym. Sci.* 110 (1998) 263.
- [29] B.S. Murray, B. Cattin, E. Schüler, Z.O. Sonmez, *Langmuir* 18 (2002) 9476.
- [30] T.G. Mason, J. Bibette, *Phys. Rev. Lett.* 77 (1996) 3481.
- [31] J. Bibette, *J. Colloid Interface Sci.* 147 (1990) 474.
- [32] O.D. Velev, B.E. Campbell, R.P. Borwankar, *Langmuir* 14 (1998) 4122.
- [33] E. Leclerc, P. Calmettes, *Phys. Rev. Lett.* 78 (1997) 150.
- [34] T. Nylander, M.N. Wahlgren, *Langmuir* 13 (1997) 6219.

- [35] H.C. van der Mei, S. Meijer, H.J. Busscher, *J. Colloid Interface Sci.* 205 (1998) 185.
- [36] J.P. Gallinet, B. Gauthier-Manuel, *Colloid Surface* 68 (1992) 189.
- [37] G. Narsimhan, *Colloid Surface* 62 (1992) 41.
- [38] J.N. Israelachvili, H.J. Wennerström, *J. Phys. Chem.* 96 (1992) 520.
- [39] J.R. Lu, T.J. Su, R.K. Thomas, *J. Colloid Interface Sci.* 213 (1999) 426.
- [40] H. Fitzpatrick, P.F. Luckham, S. Eriksen, K. Hammond, *Colloid Surface* 65 (1992) 43.
- [41] A.R. Mackie, P. Gunning, P. Wilde, V. Morris, *Langmuir* 16 (2000) 2242.